INTERNAL ENERGY OF HIGH-DENSITY HYDROGEN: ANALYTIC APPROXIMATIONS COMPARED WITH PATH INTEGRAL MONTE CARLO CALCULATIONS

S. A. Trigger [a], ***W. Ebeling*** [a], ***V. S. Filinov*** [b*],
V. E. Fortov [b], ***M. Bonitz*** [c **]

[a] *Institut für Physik, Humboldt-Universität Berlin*
D-10115, Berlin, Germany

[b] *Institute for High Energy Density, Russian Academy of Sciences*
127412, Moscow, Russia

[c] *Fachbereich Physik, Universität Rostock*
D-18051, Rostock, Germany

Submitted 30 September 2002

The internal energy of high-density hydrogen plasmas in the temperature range $T = 10000 \ldots 50000$ K is calculated by two different analytic approximation schemes — the method of an effective ion–ion interaction potential and the Padé approach within the chemical picture — and are compared with the direct path integral Monte Carlo results. A reasonable agreement between the results obtained from the three independent calculations is found and the reasons for still existing differences are investigated. Interesting high-density phenomena such as the onset of ion crystallization are discussed.

PACS: 52.25.Kn, 52.65.Pp

1. INTRODUCTION

Thermodynamics of strongly correlated Fermi systems at high pressure is of growing importance in many fields, including shock and laser plasmas, astrophysics, solids, and nuclear matter, see Refs. [1–6] for an overview. In particular, the thermodynamic properties of hot dense plasmas are essential for the description of plasmas generated by strong lasers [5]. Further, among the phenomena of current interest are the high-pressure compressibility of deuterium [7], metallization of hydrogen [8], plasma phase transition etc., which occur in situations where both interaction and quantum effects are relevant. Among the early theoretical papers on dense hydrogen we refer to Wigner and Huntington [9], Abrikosov [10], Ashcroft [11], and Brovman et al. [12]; concerning the plasma phase transition, see Norman and Starostin [13], Kremp et al. [14], Saumon and Chabrier [15], and Schlanges et al. [16], and also some earlier investigations of one of us [17–20]. Among the early simulation approaches, we refer to several Monte Carlo calculations, e.g., [21–23].

There has been significant progress in recent years in studying these systems analytically and numerically, see, e.g., [1, 2, 4, 24–28] for an overview. But there remains an urgent need to test analytic models by an independent numerical approach. In addition to the molecular dynamics approach, e.g. [24, 26], the path integral Monte Carlo (PIMC) method is particularly well suited to describe thermodynamic properties in the high-density region. This is because it starts from the fundamental plasma particles, electrons and ions, (physical picture) and treats all interactions, including bound state formation, rigorously and selfconsistently. We note a remarkable recent progress in applying these techniques to Fermi systems, see, e.g., Refs. [1, 2, 29, 30] for an overview.

Several methods have been developed to perform

*E-mail: filinov@ok.ru
**E-mail: bonitz@physik.uni-rostock.de

quantum Monte Carlo calculations. We first mention the restricted PIMC method (RPIMC) [31–34], where special assumptions on the density operator $\hat{\rho}$ are introduced in order to reduce the sum over permutations to even (positive) contributions only. It can be shown, however, that this method does not reproduce the correct ideal Fermi gas limit [35]. An alternative is given by direct fermionic PIMC simulations (DPIMC), which have occasionally been attempted by various groups, see, e.g., [36, 37] and references therein. But these simulations have been very inefficient because of the fermionic sign problem. Recently, three of us proposed a new path integral representation for the N-particle density operator [38–41] that allows direct fermionic path integral Monte Carlo simulations of dense plasmas in a wide range of densities and temperatures. Using this concept, the pressure and energy of a degenerate strongly coupled hydrogen plasma [39–42] and the pair distribution functions in the partial ionization and dissociation region [40, 41] have been computed. This scheme is rather efficient when the number of time slices (beads) in the path integral is less than or equal to 50 and was found to work well for temperatures $k_B T > 0.1\,\mathrm{Ry}$.

One difficulty of PIMC simulations is that reliable error estimates are often not available, in particular for strongly coupled degenerate systems. Here, we make a comparison with two independent analytic methods. The first is the method of an effective ion–ion interaction potential (EIIP) that has previously been developed for application to simple solid and liquid metals [12, 24] and which is here adopted to dense hydrogen for the first time. The second is the method of Padé approximations in combination with Saha equations, i.e., the chemical picture (PACH) [3]. The Padé formulas are constructed on the basis of the known analytic low-density [3, 43] and high-density [3] limits and are exact up to quadratic terms in the density, interpolating between the virial expansions and the high-density asymptotic regime [19, 44, 45].

We show here that both methods, EIIP and PACH, provide results for the internal energy that agree well with each other at high-densities where the electrons are strongly degenerate and no bound states exist, approximately for $n > 10^{24}$ cm^{-3}. In this region, there is also a good agreement with recent density functional results [46]. The agreement of the PACH and DPIMC results is good below 10^{22} cm^{-3}. For intermediate densities, where the ionization degree changes strongly, we observe deviations. Also, at high-densities, the DPIMC results tend to lower energies than the analytic approaches. Finally, they reveal several interesting effects, such as the formation of clusters and the onset of ion crystallization.

2. PHYSICAL PARAMETERS AND BASIC EFFECTS

We study a hydrogen plasma consisting of N_e electrons and N_p protons ($N_e + N_p = N$). The total proton (atom) density is $n = N_p/V$. The average distance between the electrons is the Wigner–Seitz radius

$$d = \left(\frac{3}{4\pi n}\right)^{1/3},$$

and other characteristic lengths are the Bohr radius

$$a_B = \frac{\hbar^2}{me^2},$$

the Landau length

$$l = \frac{e^2}{kT},$$

and the De Broglie wave length

$$\Lambda_e = \frac{h}{(2\pi m_e kT)^{1/2}}$$

of the electrons. The degeneracy parameter is $n\Lambda_e^3$. We define the dimensionless temperature $\tau = kT/\,\mathrm{Ry}$, which varies between $0.06 < \tau < 0.4$ in the temperature interval considered below. We also introduce the Wigner–Seitz parameter

$$r_s = \frac{d}{a_B}$$

and the dimensionless classical coupling strength

$$\Gamma = \frac{e^2}{kTd}.$$

Hydrogen is antisymmetric with respect to the charges ($e_- = -e_+$) and symmetric with respect to the densities ($n_+ = n_- = n$). Ions and electrons behave quite differently because of the big mass difference, $m_p = 1836\ m_e$. At the temperatures considered, the ions can be treated classically as long as $n \lesssim 10^{27}$ cm^{-3}. For these temperatures and densities, the proton coupling parameter is in the range $0 < \Gamma < 150$, and we can therefore expect strong coupling effects. We study internal energies of the fluid hydrogen system and start with providing some simple estimates for guidance. In that follows, we give all energies in Rydberg units.

First, at very low densities, the electrons and protons behave like an ideal Boltzmann gas. Therefore,

the energy (of free electrons and protons) per proton is given by

$$\epsilon = E/N = 3\tau. \tag{1}$$

In other words, the low-density limit is, in our temperature interval, a positive number in the region $\epsilon \approx$ $\approx$ 0.2–1.2. With increasing the density, we expect a region where atoms and possibly also a few molecules are formed [17, 41]. In the region of atoms, a lower bound for the energy per proton is

$$\epsilon = \frac{3}{2}\tau - 1, \tag{2}$$

where the last term represents the binding energy 1 Ry of H-atoms. If molecules are formed, the corresponding estimate per proton is lower,

$$\epsilon = \frac{3}{4}\tau - 1.17. \tag{3}$$

Generally, the existence of a lower bound for the energy per proton was proven by Dyson and Lenard [47] and Lieb and Thirring [48],

$$E/N > -C, \tag{4}$$

where the best estimate known to us (which is certainly much too large) is $C \approx 23$ [48]. We see that with increasing the density, the energy per proton tends to negative values and can reach a finite minimum. Further density increase causes the energy to increase again as a result of quantum degeneracy effects.

To understand this increase, we first consider the limit of a very high-density (but in the region where the protons are classical). Then the first estimate of the energy is

$$\epsilon = \frac{3}{2}\tau + \frac{2.21}{r_s^2}, \tag{5}$$

which is positive. The last term, representing the Fermi energy of the electrons, strongly increases with the density (as $n^{2/3}$). In the next approximation, according to Wigner's estimate [49][1)], we must take the Hartree contribution to the electron energy and the corresponding estimate for the proton energy into account. The latter is estimated under the assumption that the protons form a lattice. This way, we find the estimate

$$\epsilon = \left(\frac{3}{2}\tau - \frac{0.8755}{r_s}\right) + \left(\frac{2.21}{r_s^2} - \frac{0.916}{r_s}\right). \tag{6}$$

[1)] Wigner's original estimate for the lattice energy was lateron corrected, and we use an improved result. For a discussion of various estimates, see, e.g., chapter V of G. D. Mahan, *Many-Particle Physics*, Plenum Press (1990).

The two corrections that were added to Eq. (5) are both negative and scale as $n^{1/3}$. In other words, these interaction terms might play a major role with decreasing the density. At a critical density, the energy per proton can become negative. This density can be estimated from Eq. (6) by solving the quadratic equation

$$0 = \frac{3}{2}\tau\, r_s^2 - 1.7915\, r_s + 2.21 \tag{7}$$

perturbatively, starting with the zero temperature limit, and adding the first correction (linear in τ),

$$r_s^0 \approx 1.234 + 2.283\tau + \ldots \tag{8}$$

As $\tau \to 0$, this result coincides with Wigner's criterion for the existence of molecules: for $d < a_B$, molecules cannot exist because there is no room for forming bound state wave functions. According to Eq. (8), molecules exist at a finite temperature only for larger d as thermal fluctuations increase the wave function overlap. More generally, with increasing the temperature, the energy becomes positive at lower density compared to the case where $T = 0$.

Summarizing the qualitative results obtained in this section, we can state that we expect the following general behavior of the internal energy per proton in the given temperature range: at zero density, the energy starts with the ideal gas expression that depends only on the temperature. With increasing the density, the energy per proton becomes negative because of correlation effects (bound states, electron correlations, and proton correlations). A minimum is formed and at a density where the proton density is close to the inverse Bohr radius cubed, the energy per proton turns to positive values and is more and more determined by the ideal electron energy increasing with $n^{2/3}$, corrected by correlation contributions of the order $n^{1/3}$ determined by the Hartree term and by proton–proton coupling effects. In what follows, we show that this qualitative picture is supported by the results of our calculations.

3. THE METHOD OF AN EFFECTIVE ION–ION INTERACTION POTENTIAL

It is well known that in plasmas and plasma-like systems, in a broad parameter range, the interaction between the electron and ion subsystems is weak, whereas the interacrtions within the electron and ion subsystems can be strong. The corresponding small parameter is the ratio u_{ei}/E_F of the characteristic value of the electron–ion interaction u_{ei} to the electron Fermi energy E_F. Therefore, the approximation of a small

u_{ei}/E_F ratio is valid for systems with degenerate electrons if $E_F \gg T_e \geq T_i$, where T_e and T_i are the electron and ion temperatures respectively (below, we consider the case where $T_e = T_i$). Typical systems where this approximation is applicable are simple solid and liquid metals and nontransitional metals in general; and this approximation serves as the basis for the computation of thermodynamic and electron kinetic properties, see, e.g., [24, 50].

For simple metals, the Fermi energy is not very large compared with the characteristic electron–ion Coulomb interaction taken at the average interparticle distance. But because the wave functions for the conduction electrons and the electrons bound in the ion shells are orthogonal, a partial compensation of the electron–ion Coulomb attraction occurs at small distances, which effectively weakens the electron–ion interaction. This fact is described in the theory of simple metals in the framework of the so-called pseudopotential theory. The calculation of the pseudopotential is a complicated problem in general, in particular due to its nonlocal structure [50, 51]. For practical applications, it can be represented approximately as a local interaction with one or two fitting parameters for each metal. On basis of the pseudopotential theory, all thermodynamic properties and electron kinetic coefficients can be calculated with sufficiently high accuracy for a wide range of temperatures and pressures. Naturally, these calculations require a reliable knowledge of the properties of the two quasi-independent subsystems: the degenerate electron liquid in the positive charge background and the classical ion subsystem with some effective strong inter-ion interaction.

It is apparent that there is also a wide range of parameters for highly ionized strongly compressed hydrogen plasmas where the electron–ion interaction is weak. For these parameters, the complicated problem of calculating the properties of a strongly coupled quantum electron–proton system can be essentially simplified. In so doing, the results obtained for high compression (when no bound electron states — hydrogen atoms or molecules — exist), do not require any fitting, in contrast to the case of simple metals, because the inter-ion potential for hydrogen is a purely Coulomb one. The data obtained with this analytic approximation can therefore be considered as a reliable basis for comparison with the results of alternative approaches, including analytic and simulation methods for degenerate quantum systems of Fermi particles. The results of this pseudopotential approach are especially important for conditions of the extreme compression where the plasma is characterized by a strong interaction within the electron and especially the ion subsystem. For these difficult situations, experimental data are still missing and new accurate numerical methods for Fermi system are only emerging.

We consider the Hamiltonian of an electron–proton plasma, where the $q = 0$ infinite contributions to the potentials cancel because of quasineutrality (and we retain the charge number Z of the ions for generality),

$$H = \sum_k \epsilon_k a_k^\dagger a_k + \frac{1}{2V} \sum_{k,k',q\neq 0} \frac{4\pi e^2}{q^2} a_{k-q}^\dagger a_{k'+q}^\dagger a_{k'} a_k + \\ + \frac{1}{V} \sum_{k,q'\neq 0} u_{ei}(q) a_k^\dagger a_{k+q} \sum_{j=1}^{N_i} \exp(i\mathbf{q}\cdot\mathbf{R}_j) + \\ + \frac{1}{2V} \sum_{i\neq j} \sum_{q\neq 0} \frac{4\pi Z^2 e^2}{q^2} \exp(i\mathbf{q}\cdot(\mathbf{R}_i - \mathbf{R}_j)) + K_i. \quad (9)$$

Here, ϵ_k is the energy of the electron with the momentum $\hbar k$ and

$$u_{ei}(q) = -\frac{4\pi Z e^2}{q^2}$$

is the Fourier component of the electron–proton interaction potential. For the electron degrees of freedom in the Hamiltonian H, the representation of second quantization is used, with $a_p^\dagger$ and a_p being the respective creation and annihilation operators of an electron with momentum p. For classical ions, the coordinate representation is more convenient, and R_i therefore denotes the coordinate of the i-th ion in Eq. (9). As in the theory of simple metals [12, 24], two main approximations have to be used to calculate the plasma energy. The first is the adiabatic approximation for the ion motion, which is slow compared to the electron one. The second is the smallness of the ratio of the characteristic electron–proton Coulomb interaction to the Fermi energy E_F. The respective parameter is

$$\Gamma_{ei} = \frac{Ze^2}{dE_F} = Z\Gamma\frac{kT}{E_F} \propto n^{-1/3}.$$

Calculation of the electron energy in the external field of immobile ions (protons) leads to the energy of the plasma given as function of the ion coordinates R_j. In general, the perturbation theory in terms of the parameter Γ_{ei} gives rise not only to pair but also to higher-order ion–ion interactions, which are quite complicated. To the second order of perturbation theory in the parameter Γ_{ei}, the energy per one electron of a plasma

with a fixed proton configuration $\{R_j\}$ is easily written as

$$\frac{E\left(\{R_j\}\right)}{N_i} = \frac{\langle H\rangle_e}{N_i} = \epsilon_e + \frac{3}{2}kT - \\ - \frac{1}{2}\int \frac{d^3q}{(2\pi)^3}\frac{u_{ei}^2(q)\Pi_e(q)}{\varepsilon_e(q)} - \\ - \frac{Z^2 n_i}{2\Pi_e(q=0)} + \frac{1}{2VN_i}\sum_{\mathbf{q}}\sum_{i\neq j}\mathcal{V}^{eff}(q)\times \\ \times \exp(i\mathbf{q}\cdot(\mathbf{R}_i - \mathbf{R}_j)), \quad (10)$$

where ϵ_e is the energy (per ion) of the correlated electron liquid in the homogeneous positive charge background. The respective functions $\Pi_e(q)$ and $\varepsilon_e(q)$ are the static polarization function and the static dielectric function of the correlated electron liquid. They are related by the usual equality

$$\varepsilon_e(q) = 1 + \frac{4\pi e^2}{q^2}\Pi_e(q). \quad (11)$$

The Fourier component of the effective pair interaction potential between the ions, $\mathcal{V}_{ii}^{eff}$, involved in (10) is given by

$$\mathcal{V}_{ii}^{eff}(q) = \frac{4\pi Z^2 e^2}{q^2} - u_{ei}^2(q)\frac{\Pi_e(q)}{\varepsilon_e(q)} = \frac{4\pi Z^2 e^2}{q^2\varepsilon_e(q)}. \quad (12)$$

In what follows, we concentrate on hydrogen and set $Z = 1$, which leads to the effective proton–proton interaction

$$\mathcal{V}_{pp}^{eff}(q) = \frac{4\pi e^2}{q^2\varepsilon_e(q)}. \quad (13)$$

It is clear that in contrast to liquid metals, where the presence of the pseudopotential leads to a more complicated structure of the effective potential, in a dense hydrogen plasma, the effective potential is determined only by the electron screening. As shown in [12] for liquid metals, the additional pair interaction arising from third- and fourth-order terms in the expansion of the electron energy in the pseudopotential can play an important role in the effective interaction. A detailed analysis of the effective potential of a hydrogen plasma [52] revealed that these terms are essential only for sufficiently rarified plasma conditions ($r_s > 1.5$) and are practically negligible for higher densities, $r_s < 1.5$, which we consider in this paper. In fact, for $r_s > 1.6$, the structure of the effective ion–ion potential in hydrogen changes drastically and can be considered as a precursor of the appearence of molecular states. In this paper, we use the simplest version of the method of an effective ion–ion potential that includes the electron–proton interaction up to the second order, and we are therefore restricted to sufficiently high-densities corresponding to $r_s < 1.5$.

Further progress can be made using the random phase approximation (RPA) for Π_e together with the long-wavelength and short-wavelength limits,

$$\Pi^{RPA}(q) = \\ = \begin{cases} \Pi^{RPA}(0)\left[1 - \dfrac{1}{12}\dfrac{q^2}{q_F^2}\right], & q \ll q_F, \\ \Pi^{RPA}(0)\dfrac{4}{3}\dfrac{q_F^2}{q^2}, & q \gg q_F, \end{cases} \quad (14)$$

where $\hbar q_F = \sqrt{2m\epsilon_F}$ is the Fermi momentum of the electrons. The analysis of this expression shows that the main contribution to energy (10) comes from small wave numbers[2)]. With sufficient accuracy, we can therefore neglect the q dependence of Π_e in Eq. (10) and, in particular, in effective potential (12), replacing

$$\Pi^{RPA}(q) \to \Pi^{RPA}(0).$$

This implies that we also neglect the well-known small oscillations of the effective potential for large distances, which are the result of a logarithmic singularity of the derivative

$$\left.\frac{d\Pi^{RPA}}{dq}\right|_{q=2q_F}.$$

For the densities under consideration (which are much higher than the usual metallic densities), these oscillations are not essential for the thermodynamic functions. On the other hand, it is crucial to calculate the polarization function $\Pi_e(0)$ fully selfconsistently,

$$\Pi_e(0) = \left(\frac{\partial n}{\partial \mu_e}\right)_{T,V}, \quad \mu_e = \left(\frac{\partial n\epsilon_e}{\partial n}\right)_{T,V}, \quad (15)$$

where ϵ_e is determined by (10) and consequently takes the electron–electron exchange and correlations into account. In the case of degenerate electrons, we can use one of the analytic approximations for ϵ_e such as, for example, that of Nozieres and Pines or Wigner, see, e.g., [53] for an overview. Below, we use Wigner's formula for the correlation energy, although the approximation of Nozieres and Pines is better for small r_s (in the region $r_s < 1$, where the deviations between these approximations for the correlation energy become essential, we can completely neglect correlations in comparison to the kinetic and exchange terms). Because

$$\Pi_e^{RPA}(0) = \frac{\kappa_{TF}^2}{4\pi e^2},$$

[2)] As was shown by [52], for hydrogen at $r_s < 1.6$ (which we will apply the EEIP method to) the contribution of nonzero wavenumbers is comparatively small. For $r_s > 1.65$, however, the situation starts to change drastically.

it is clear that Eq. (15) implies renormalization $\Pi_e^{RPA} \to \Pi_e$ due to the electron–electron interaction, and therefore, a renormalization of the momentum $\kappa_{TF} \to \tilde{\kappa}_{TF}$,

$$\Pi_e(0) = \Pi_e^{RPA}(0)\,\gamma(r_s), \quad \tilde{\kappa}_{TF} \equiv \kappa_{TF}\sqrt{\gamma(r_s)},$$
$$\gamma(r_s) = \left(\frac{9\pi}{4}\right)^{2/3} \frac{6}{r_s^2}\left[r_s^2\frac{\partial^2\epsilon_e}{\partial r_s^2} - 2r_s\frac{\partial\epsilon_e}{\partial r_s}\right]^{-1}. \qquad (16)$$

Because the effective proton–proton potential is described by the screened potential of the Thomas–Fermi type, in the considered approximation, see Eqs. (12)–(16),

$$\Phi_{pp}(r) = \frac{e^2}{r}\exp\left(-\frac{r}{\tilde{r}_{TF}}\right), \qquad (17)$$

we conclude that a renormalization of the screening radius due to electronic correlations occurs

$$\tilde{r}_{TF} = \frac{1}{\tilde{\kappa}_{TF}} \equiv \frac{r_{TF}}{\sqrt{\gamma(r_s)}}. \qquad (18)$$

We now rewrite Eg. (10) for the considered approximation as

$$\epsilon = \epsilon_e + \epsilon_i, \qquad (19)$$

$$\epsilon_i = \frac{3}{2}kT + \frac{1}{2N}\sum_{i\neq j}\Phi_{pp}(R_i - R_j) - \\ - \frac{e^2}{d}\left(\frac{\kappa}{2} + \frac{3}{2\kappa^2}\right), \qquad (20)$$

where $\kappa \equiv d\tilde{\kappa}_{TF}$. After averaging over the proton positions with the Gibbs distribution (denoted by $\langle \ldots \rangle$), Eq. (19) can be represented as the sum of two terms: the energy ϵ_e of a degenerate electron liquid in the positive homogeneous charge background and the energy of screened classical charged protons interacting via screened potential (18) and renormalized by the constant terms obtained above,

$$\epsilon_i = \left(u + \frac{3}{2}\right)kT, \qquad (21)$$

with

$$u \equiv \Gamma\left\{\frac{d}{2Ne^2}\left\langle\sum_{i\neq j}\Phi_{pp}(R_i - R_j)\right\rangle - \frac{\kappa}{2} - \frac{3}{2\kappa^2}\right\}. \qquad (22)$$

Here, u is the ionic interaction energy in kT units. With the accuracy $(kT/E_F)^2$, energy (21) coincides with the usual thermodynamic energy determined from the free energy of the system because the electrons are degenerate in the considered parameter range (with the same accuracy). Expression (21) implies that the energy of a classical one-component system of charged particles interacting via a screened (Debye or Yukawa) potential tends to infinity as $3k_BT\Gamma/2\kappa^2$ for $\kappa \to 0$ (i.e., the screening radius diverges). As a function of the two parameters, Γ and the dimensionless screening length κ, the function u/Γ has been tabulated in [54, 55] for the calculations of the phase diagram of a purely classical one-component Debye plasma (OCP), based on accurate MC calculations for the Debye system. Below, we use these numerical results to calculate the energy of a dense hydrogen plasma in the above approximations. Within the Wigner approximation for the electron energy,

$$\epsilon_e = \left(\frac{2.21}{r_s^2} - \frac{0.916}{r_s} + \epsilon_{corr}\right)\mathrm{Ry}, \\ \epsilon_{corr} = -\frac{0.88}{r_s + 7.8}, \qquad (23)$$

we obtain from Eq. (16) that

$$\gamma(r_s) = \frac{22.1}{r_s^2\varphi(r_s)}, \\ \varphi(r_s) = \frac{22.1}{r_s^2} - \frac{3.664}{r_s} - \frac{1.76r_s}{(r_s+7.8)^2} - \frac{1.76r_s^2}{(r_s+7.8)^3}, \qquad (24)$$

where $\gamma(r_s \to 0) \to 1$. The total internal energy in Eq. (21) can now be expressed in terms of the tabulated function u/Γ as

$$\epsilon = \left[\frac{2.21}{r_s^2} - \frac{0.916}{r_s} + \epsilon_{corr} + \frac{2}{r_s}\left(\frac{u}{\Gamma} + \frac{3}{2\Gamma}\right)\right]\mathrm{Ry}. \qquad (25)$$

The numerical results computed from this approximation are included in Figs. 1–3 below.

Alternatively, we can use additional approximations for the computation of the internal energy of the plasma. This can be done by averaging Eq. (10) over the ion Gibbs distribution with the same effective Hamiltonian. We then immediately find the average energy per proton

$$\frac{\langle E\{R_i\}\rangle}{N_p} = \epsilon_e + \frac{3}{2}k_BT - \frac{1}{2}\int\frac{d^3q}{(2\pi)^3}\frac{u_{ei}^2(q)\Pi_e(q)}{\varepsilon_e(q)} + \\ + \frac{1}{2}\int\frac{d^3q}{(2\pi)^3}\mathcal{V}_{ii}^{eff}(q)\,[S_{ii}(q) - 1] = \\ = \epsilon_e + \frac{3}{2}k_BT + \frac{1}{2}\int\frac{d^3q}{(2\pi)^3}u_{ii}(q)\,[S_{ii}(q) - 1] - \\ - \frac{1}{2}\int\frac{d^3q}{(2\pi)^3}\frac{u_{ei}^2\Pi_e(q)}{\varepsilon_e(q)}S_{ii}(q), \qquad (26)$$

where we introduced the ion–ion structure factor $S_{ii}(k)$ defined as

$$\langle \varrho_{\mathbf{k}_1} \varrho_{\mathbf{k}_2} \rangle = N S_{ii}(\mathbf{k}_1) \delta_{\mathbf{k}_1+\mathbf{k}_2,0} + N^2 \delta_{\mathbf{k}_1,0} \delta_{\mathbf{k}_2,0},$$

$$\varrho_{\mathbf{k}} \equiv \sum_j \exp(-i\mathbf{k}\cdot\mathbf{R}_j), \quad \delta_{\mathbf{k},0} = \begin{cases} 1, & k = 0, \\ 0, & k \neq 0. \end{cases} \tag{27}$$

Equation (26) can be simplified by replacing, approximately, the full structure factor by the OCP structure factor S_{ii}^{OCP} computed with the effective ion–ion interaction. The total energy can then be written as the sum of three contributions: the first from the electron subsystem, the second from the classical ion OCP subsystem (each imbedded into a positive and negative charge background respectively), and a third term ϵ_i^{POL} that describes a perturbation-theory approximation for the polarization of the electron liquid by the ions. The resulting formulas coincide with the perturbation approximations derived by Hansen, De Witt, and others [22, 23],

$$\frac{\langle E\{R_i\}\rangle}{N_p} = \epsilon_e + \epsilon_i^{OCP} + \delta\epsilon\,, \tag{28}$$

$$\delta\epsilon = \frac{e^2}{\pi} \int_0^\infty dq \left(\frac{1}{\varepsilon_e(q)} - 1 \right) S_{ii}^{OCP}(q). \tag{29}$$

As is clear from the above derivations, Eqs. (28) and (29) are less accurate than the full EIIP model presented above.

4. PADÉ APPROXIMATIONS AND CHEMICAL PICTURE: THE PACH METHOD

In this section, we briefly explain the method of Padé approximations in combination with the chemical picture, i.e., Saha equations [3, 19, 44, 45] (PACH). On the basis of the PACH approximation, we calculate the internal energy for the three isotherms $T = 10000$, 30000, and 50000 K. This method works with only analytical formulas, which are rather complicated, however; nevertheless, the calculation of one energy data point takes no more than a few seconds on a PC.

The Padé approximations were constructed in earlier works from the known analytic results in the limiting cases of low density [3, 43] and high-density [3]. The structure of the Padé approximations was devised such that they are analytically exact up to quadratic terms in the density (up to the second virial coefficient) and interpolate between the virial expansions and the high-density asymptotic expressions [19, 44, 45]. The formation of bound states was taken into account using the chemical picture.

We here follow this cited work in large part, only the contribution of the OCP-ion–ion interaction, which is the largest one in most cases, was substantially improved following [56]. With respect to the chemical picture, we restricted ourselves to the strong ionization region, where the number of atoms is still relatively low and no molecules are present. We here discuss only the general structure of the Padé formulas. The internal energy density of the plasma is given by

$$E = E_{id} + E_{int}, \tag{30}$$

where E_{id} is the internal energy of an ideal plasma consisting of Fermi electrons, classical protons, and classical atoms and

$$E_{int} = N_p \left(\epsilon_e + \epsilon_i + \epsilon_a\right) \tag{31}$$

is the interaction energy. The splitting of the interaction contribution to the internal energy corresponds largely to the previous section. The individual pieces are as follows.

1) The electron–electron interaction ϵ_e. This term corresponds to the OCP energy of the electron subsystem. Instead of the simple expressions used in earlier work [19, 42, 44], we here used a more refined formula for the energy [57]. This formula is an interpolation between the Hartree limit with the Gellman–Brueckner correction (already used in the previous section), the Wigner limit, and the Debye law including quantum corrections,

$$\epsilon_e = -\frac{(r_s^3+50)\left[a_H + a_W(r_s)\right] + 2\sqrt{6}d_0 r_s^{5.5}\tau^{2.5} + 24 d_H r_s^4 \tau^2}{(r_s^3+50)r_s + 2.3 r_s^4\tau^2 + 2\sqrt{6}d_1 r_s^{5.5}\tau^2 + r_s^7\tau^3}. \tag{32}$$

Here, a Wigner function has been introduced as

$$a_W(x) = 2b_0 x \times \\ \times \ln\left(1 + \left[x^{0.5}\exp\left(-\frac{b_1}{2b_0}\right) + \frac{2b_0 x}{a_W}\right]^{-1}\right), \quad (33)$$

and the constants take the values

$$d_0 = 0.5, \quad d_1 = 0.6631, \quad d_H = 0.125,$$

$$a_H = 0.91633, \quad a_W = 0.87553,$$

$$b_0 = 0.06218, \quad b_1 = 0.0933.$$

We mention that similar formulas are also valid for other thermodynamic functions with the constants adjusted [57]. The formula for the OCP used here contains all the terms taken into account in the previous section and in addition, also temperature-dependent corrections.

2) The ion contribution to the internal energy ϵ_i. This term was calculated in the previous section. We here use a procedure based on approximation (28), (29). This enables us to use the results of the MC calculations of Hansen, De Witt, and others [23, 58]. In accordance with Eqs. (28) and (29), the ion contribution is split into two terms,

$$\epsilon_i = \epsilon_i^{OCP} + \epsilon_i^{POL}, \quad (34)$$

where the first is the OCP contribution of the protons and the second represents the polarization of the proton OCP by the electron gas. For the region of high densities, i.e., large Γ and small r_s, we use the Monte Carlo data that were parametrized by De Witt as [23]

$$\epsilon_i^{OCP} = -0.8946\Gamma + 0.8165\Gamma^{0.25} - 0.5012, \quad (35)$$

$$\epsilon_i^{POL} = -r_s(0.0543\Gamma + 0.1853\Gamma^{0.25} - 0.0659). \quad (36)$$

We note that the polarization term describes the correction due to screening of the proton–proton interaction by the electron fluid. In order to obtain these expressions, semiclassical Monte Carlo calculations were performed based on effective ion interactions that model the electrons as a responding background [22, 23]. We do not need to go into the details of this method because the procedure corresponds to Eq. (29) derived in the previous section.

In the low density limit, we used the Debye law with quantum corrections [3, 45],

$$\epsilon_i^{OCP} = -0.86603\tau d_0\Gamma^{1.5}[1 - B_1\Gamma^{1.5}], \quad (37)$$

$$\epsilon_i^{POL} = -0.71744\Gamma^{1.5}[1 - C_1\Gamma^{1.5}]. \quad (38)$$

Here, the temperature functions B_1 and C_1 describe rather complex quantum corrections, which are, however, explicitly known and are easily programmed [3]. The Padé approximations that connect the high- and the low-density limits are constructed by standard methods [19, 44, 45] and are not given here explicitly. For the OCP energy of the ions, we use the very accurate formulas proposed by Kahlbaum [56].

3) The atomic contribution ϵ_a. In the region of densities and temperatures studied in this work, this contribution gives only a small correction (except for $T = 10000$ K). We calculate the number of atoms on the basis of a nonideal Saha equation described below. The formation of molecules is not taken into account. We restrict the calculations to a region where the number density of atoms is smaller than that of the electrons. The contributions to the chemical potential that appear in the Saha equation are calculated in part from scaling relations and in part by numerical differentiation of the free energy given earlier [19, 44]. For the partition function in the Saha equation, we use the Brillouin–Planck–Larkin expression [3, 45]. The nonideal Saha equation that determines the ionization degree (the density of atoms) is solved by iterations, starting from the ideal Saha equation. Because of the high degree of ionization, the atomic interaction contributions can be approximated in the simplest way by the second virial contribution and by treating the atoms as small hard spheres and by neglecting the charged particle-neutral interaction.

The results of our Padé calculations for a broad density interval for three isotherms are included in Figs. 1–3.

5. SUMMARY OF THE PATH INTEGRAL MONTE CARLO SIMULATIONS

The analytic approximations discussed in the previous sections work very well at high densities if bound states are of minor importance. These conditions are not fulfilled for densities below the Mott point corresponding to $r_s > 1$. Here, recently developed DPIMC simulations can be used. Starting from the basic plasma particles, electrons and ions, they «automatically» account for bound state formation and ionization and dissociation. Furthermore, in contrast to the chemical picture, no restrictions on the type of chemical species are made and the appearance of complex aggregates such as molecular ions or clusters of several atoms are fully included. On the other hand, the sim-

ulations are expected to become increasingly difficult at high densities where the electron degeneracy is large due to the Fermion sign problem. It is therefore very interesting to compare results of the DPIMC approach with alternative theories that are expected to complement each other. This is done in the next section.

But first, we briefly outline the idea of our DPIMC scheme. All thermodynamic properties of a two-component plasma are defined by the partition function Z; for of N_e electrons and N_p protons, it is given by

$$\begin{aligned} Z(N_e,N_p,V,\beta) &= \frac{Q(N_e,N_p,\beta)}{N_e!N_p!}, \\ Q(N_e,N_p,\beta) &= \sum_\sigma \int\limits_V dq\, dr\, \rho(q,r,\sigma;\beta) \end{aligned} \tag{39}$$

where $\beta = 1/k_BT$. For a quantum system, the exact density matrix is not known in general, but can be constructed using a path integral representation [21, 59–61],

$$\begin{aligned} &\int\limits_V dR^{(0)} \sum_\sigma \rho(R^{(0)},\sigma;\beta) = \\ &\quad = \int\limits_V dR^{(0)} \dots dR^{(n)}\, \rho^{(1)}\rho^{(2)} \dots \rho^{(n)} \times \\ &\qquad \times \sum_\sigma \sum_P (\pm 1)^{\kappa_P}\, \mathcal{S}(\sigma,\hat{P}\sigma')\, \hat{P}\rho^{(n+1)}, \end{aligned} \tag{40}$$

where

$$\begin{aligned} \rho^{(i)} &\equiv \rho\left(R^{(i-1)},R^{(i)};\Delta\beta\right) \equiv \\ &\equiv \langle R^{(i-1)}|\exp(-\Delta\beta\hat{H})|R^{(i)}\rangle, \end{aligned}$$

with

$$\Delta\beta \equiv \frac{\beta}{n+1}, \quad \Delta\lambda_a^2 = \frac{2\pi\hbar^2\Delta\beta}{m_a} \quad a = p, e.$$

Here, $\hat{H} = \hat{K} + \hat{U}_c$ is the Hamilton operator containing the kinetic and potential energy contributions, $\hat{K}$ and $\hat{U}_c$, respectively, with

$$\hat{U}_c = \hat{U}_c^p + \hat{U}_c^e + \hat{U}_c^{ep}$$

being the sum of the Coulomb potentials between protons (p), electrons (e), and electrons and protons (ep). Further, σ comprises all particle spins and the particle coordinates are denoted by

$$\begin{aligned} R^{(i)} &= (q^{(i)},r^{(i)}) \equiv (R_p^{(i)},R_e^{(i)}), \quad i = 1,\dots n+1, \\ R^{(0)} &\equiv (q,r) \equiv (R_p^{(0)},R_e^{(0)}), \quad R^{(n+1)} \equiv R^{(0)}, \end{aligned}$$

where q and r denote the electron and proton coordinates, respectively and

$$\sigma' = \sigma.$$

The particles are then represented by fermionic loops with the coordinates (beads)

$$[R] \equiv [R^{(0)}; R^{(1)}; \dots; R^{(n)}; R^{(n+1)}].$$

The spin gives rise to the spin part of the density matrix $\mathcal{S}$, and the exchange effects are taken into account by the permutation operator $\hat{P}$ that acts on the electron coordinates and spin projections and by the sum over permutations with the parity κ_P. In the fermionic case (minus sign), the sum contains $N_e!/2$ positive and negative terms, which leads to the notorious sign problem. Because of the large mass difference of electrons and ions, the exchange of the latter is not included.

Thermodynamic functions are given by derivations of the logarithm of the partition function with respect to thermodynamic variables. In particular, the internal energy E follows from Q by

$$\beta E = -\beta\frac{\partial \ln Q}{\partial\beta}, \tag{41}$$

which gives (cf. [42] for details)

$$\begin{aligned} \beta E &= \frac{3}{2}(N_e+N_p) + \frac{1}{Q}\,\frac{1}{\lambda_p^{3N_p}\Delta\lambda_e^{3N_e}} \times \\ &\times \sum_{s=0}^{N_e} \int dq\, dr\, d\xi\, \rho_s(q,[r],\beta) \times \\ &\times \left\{ \sum_{p<t}^{N_p} \frac{\beta e^2}{|q_{pt}|} + \sum_{l=0}^{n} \left[\sum_{p<t}^{N_e} \frac{\Delta\beta e^2}{|r_{pt}^l|} + \sum_{p=1}^{N_p}\sum_{t=1}^{N_e} \Psi_l^{ep} \right] + \right. \\ &+ \sum_{l=1}^{n} \left[-\sum_{p<t}^{N_e} C_{pt}^l \frac{\Delta\beta e^2}{|r_{pt}^l|^2} + \sum_{p=1}^{N_p}\sum_{t=1}^{N_e} D_{pt}^l \frac{\partial\Delta\beta\Phi^{ep}}{\partial|x_{pt}^l|} \right] - \\ &\left. - \frac{1}{\det||\psi_{ab}^{n,1}||_s}\,\frac{\partial\det|\psi_{ab}^{n,1}|_s}{\partial\beta} \right\}, \\ C_{pt}^l &= \frac{\langle r_{pt}^l|y_{pt}^l\rangle}{2|r_{pt}^l|}, \quad D_{pt}^l = \frac{\langle x_{pt}^l|y_p^l\rangle}{2|x_{pt}^l|}, \end{aligned} \tag{42}$$

where

$$\Psi_l^{ep} \equiv \Delta\beta\,\left.\frac{\partial[\beta'\Phi^{ep}(|x_{pt}^l|,\beta')]}{\partial\beta'}\right|_{\beta'=\Delta\beta}$$

contains the electron–proton Kelbg potential Φ^{ep} (cf. Eq. (45) below), $\langle\dots|\dots\rangle$ denotes the scalar product, and q_{pt}, r_{pt}, and x_{pt} are differences of the two coordinate vectors,

$$q_{pt} \equiv q_p - q_t, \quad r_{pt} \equiv r_p - r_t,$$

$$x_{pt} \equiv r_p - q_t, \quad r^l_{pt} = r_{pt} + y^l_{pt},$$
$$x^l_{pt} \equiv x_{pt} + y^l_p, \quad y^l_{pt} \equiv y^l_p - y^l_t,$$

with

$$y^n_a = \Delta\lambda_e \sum_{k=1}^{n} \xi^{(k)}_a.$$

We introduced dimensionless distances between neighboring vertices on the loop, $\xi^{(1)}, \dots \xi^{(n)}$, and thus, explicitly, $[r] \equiv [r; y^{(1)}_e; y^{(2)}_e; \dots]$. The density matrix ρ_s in Eq. (42) is given by

$$\rho_s(q,[r],\beta) = C^s_{N_e} \exp(-\beta U(q,[r],\beta)) \times \\ \times \prod_{l=1}^{n} \prod_{p=1}^{N_e} \phi^l_{pp} \det ||\psi^{n,1}_{ab}||_s, \quad (43)$$

where

$$U(q,[r],\beta) = U^p_c(q) + \frac{\{U^e([r],\Delta\beta) + U^{ep}(q,[r],\Delta\beta)\}}{n+1},$$
$$\phi^l_{pp} \equiv \exp[-\pi|\xi^{(l)}_p|^2].$$

Density matrix (43) does not involve an explicit sum over the permutations, and hence, does not involve the sum of terms with alternating signs. Instead, the whole exchange problem is contained in a single exchange matrix given by

$$||\psi^{n,1}_{ab}||_s \equiv || \exp\left\{ -\frac{\pi}{\Delta\lambda^2_e} |(r_a - r_b) + y^n_a|^2 \right\} ||_s. \quad (44)$$

As a result of the spin summation, the matrix carries a subscript s indicating the number of electrons having the same spin projection.

The potential Φ^{ab} in Eq. (42) is an effective quantum pair interaction between two charged particles immersed into a weakly degenerate plasma. It has been derived by Kelbg et al. [62, 63] who showed that it contains quantum effects exactly in the first order in the coupling parameter Γ,

$$\Phi^{ab}(|\mathbf{r}_{ab}|,\Delta\beta) = \frac{e_a e_b}{\lambda_{ab} x_{ab}} \times \\ \times \left\{ 1 - \exp(-x^2_{ab}) + \sqrt{\pi}\, x_{ab} \left[1 - \mathrm{erf}(x_{ab}) \right] \right\}, \quad (45)$$

where $x_{ab} = |\mathbf{r}_{ab}|/\lambda_{ab}$; we emphazise that the Kelbg potential is finite at zero distance.

The structure of Eq. (42) is obvious: we have separated the classical ideal gas part (the first term). The ideal quantum part in excess of the classical one and the correlation contributions are contained in the integral term, where the second line results from the ionic correlations (the first term) and the ee and ei interactions at the first vertex (the second and the third term respectively). Equation (42) therefore contains the important limit of an ideal quantum plasma in a natural way. The third and fourth lines are due to further electronic vertices and the explicit temperature dependence (Eq. (42)) and volume dependence (the corresponding equation of state) of the exchange matrix, respectively. The main advantage of Eq. (42) is that the explicit sum over permutations has been converted into the spin determinant that can be very efficiently computed using standard linear algebra methods. Furthermore, each of the sums in curly brackets in Eq. (42) is bounded as the number of vertices increases, $n \to \infty$. The error of the total expression is of the order $1/n$. Expression (42) and the analogous result for the equation of state are therefore well suited for numerical evaluation using the standard Monte Carlo techniques, see, e.g., [21, 29].

In our Monte Carlo scheme, we used three types of steps, where either electron or proton coordinates, r_i or q_i, or inidividual electronic beads $\xi^{(k)}_i$ were moved until convergence of the calculated values was reached. Our procedure has been extensively tested. In particular, we found from comparison with the known analytic expressions for the pressure and energy of an ideal Fermi gas that the Fermi statistics is very well reproduced with a limited number of particles ($N \lesssim 100$) and beads for degeneracy up to $n\lambda^3 \lesssim 10$ [40]. We also performed extensive tests for few-electron systems in a harmonic trap, where the analytically known limiting behavior (e.g. energies) is again well reproduced [64, 65]. For the present simulations of dense hydrogen, we varied both the particle number and the number of time slices (beads). As a result of these tests, we found that to obtain convergent results for the thermodynamic properties of hydrogen in the density–temperature region of interest here, particle numbers $N_e = N_p = 50$ and beads numbers in the range $n = 6 \dots 20$ are an acceptable compromise between accuracy and computational effort [39–41].

6. NUMERICAL RESULTS. COMPARISON OF THE ANALYTIC AND SIMULATION DATA

We now discuss the numerical results. We have computed the internal energy of dense hydrogen using the two analytic (EIIP and PACH) approaches and the DPIMC simulations. The data are shown in Figs. 1–3 for three temperatures, 10000, 30000, and 50000 K, respectively.

We first consider the general behavior that is most clearly seen for the highest temperature, cf. Fig. 3*a*. The overall trend is an increase of the energy with density, which is particularly rapid at high densities because of electron degeneracy effects; this is clearly seen from the ideal plasma curve (dashed and dotted lines in the lower parts of Figs. 1–3). The nonideal plasma results show a prominent deviation from this trend, which is in full agreement with the discussion in Sec. 2, the formation of an energy minimum (where the energy can become negative) at intermediate densities. Our calculations for a nonideal hydrogen plasma asymptotically approach the ideal curve both at low density (the ideal classical plasma) and at high-density (the ideal mixture of classical protons and quantum electrons). For intermediate densities, between 10^{21} and 10^{25} cm^{-3}, the nonideal plasma energy is significantly lower than the ideal energy because of strong correlations and formation of bound states. As the temperature decreases, this region broadens. In particular, we clearly see that the total energy indeed reaches negative values for the temperatures considered.

We now compare the results of the different methods. We separately consider three density regions, A) the high-density limit, B) the region around the minimum, and C) the region below the minimum.

A) The first observation from Figs. 1–3 is that for all temperatures (including temperatures above those shown), the PACH and EIIP approaches practically coincide in the limit of high densities. It is also interesting to compare these approaches with another theoretic approach based on the density functional theory (DFT). Recently, Xu and Hansen [46] published data for $T = 10000$ K and $r_s \leq 1.5$, which are also included in Fig. 1. Evidently, in the high-density limit, PACH and EIIP coincide with these DFT data, cf. Fig. 1. This good agreement of the three completely independent approaches — EIIP, PACH and DFT — is a strong indication that they can yield reliable results for a fully ionized macroscopic hydrogen plasma at high-densities. This asymptotic agreement is not surprising, because the ideal Fermi gas limit is «built into» each of these three approaches. But this gives no information about the lowest densities for which these results remain quantitatively correct. The presented comparison is therefore greatly important as giving a hint (although not a proof) that the value of that minimum density is above $n \approx 3 \cdot 10^{24}$ cm^{-3}, cf. Figs. 1–3.

We next observe that at higher densities the DPIMC simulations, yield lower energies and a shift of the energy increase to higher density values compared with the analytic models. This tendency becomes stronger with increasing the temperature, as can be seen in Figs. 1–3. In view of the asymptotic accuracy of the analytic results (see above), the total energy of macroscopic high-density hydrogen is certainly above the DPIMC results for densities exceeding 10^{25} cm^{-3}. There are two main factors tending to reduce our DPIMC results for the energies at high densities. The first factor is given by degeneracy effects. Practical limitations that must be imposed on the number of beads and particles (see Sec. 5) necessarily make our results less reliable for densities exceeding 10^{25} cm^{-3}. The second factor is given by finite-size effects related to proton ordering. To better understand the high-density results, we analyze the electron–electron (*ee*), proton–proton (*pp*) and electron–proton (*ep*) pair dis-

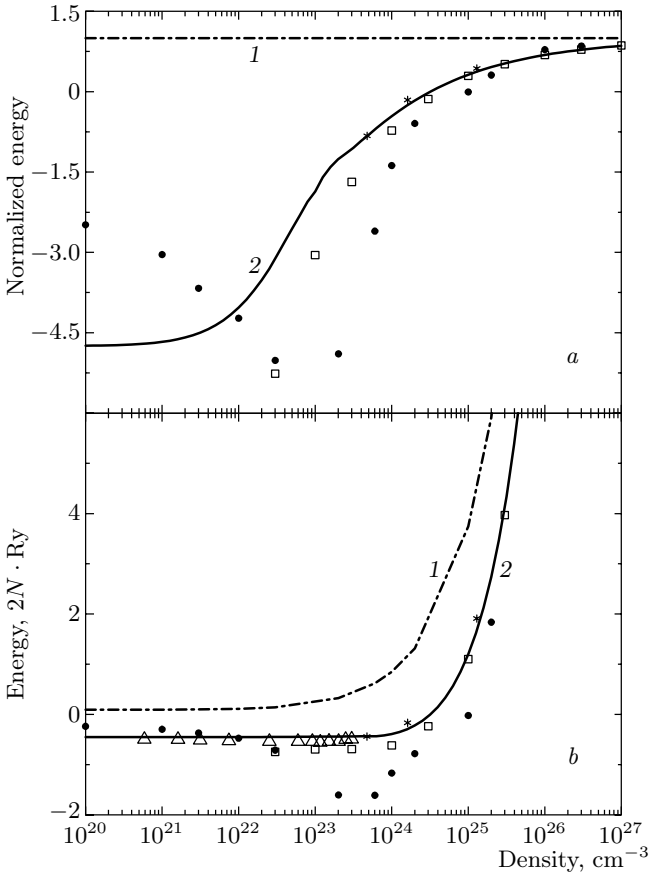

Fig. 1. Internal energy of hydrogen for $T = 10000$ K: a — normalized to the energy of a noninteracting electron–proton system; b — in the units of $2N$ Ry. The curves show the following results: ideal plasma (*1*), the PACH calculations (*2*), the EIIP model (□), our Monte Carlo simulations, DPIMC (•), density functional theory [46] (∗), and restricted PIMC data, RPIMC of Militzer et al. [34] (△)

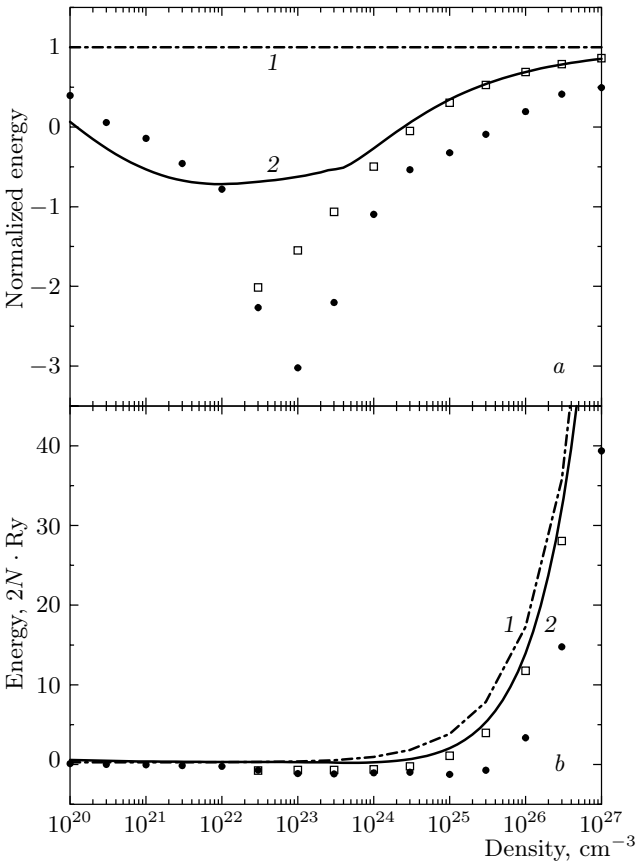

Fig. 2. Internal energy of hydrogen for $T = 30000$ K. The notation is the same as in Fig. 1

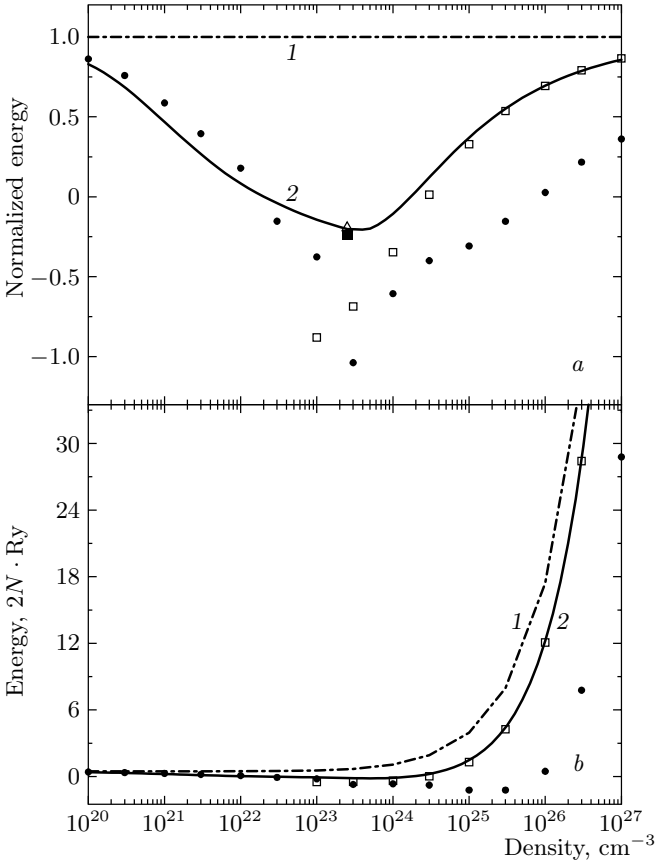

Fig. 3. Internal energy of hydrogen for $T = 50000$ K. The notation is the same as in Fig. 1

tribution functions in Fig. 4. These functions exhibit features typical for strongly correlated systems. The most prominent effect is seen in the *pp* function that exhibits a periodic structure at $T = 50000$ K, which is even more pronounced at $T = 10000$ K. This proton ordering is typical of a strongly correlated ion fluid near the crystallization temperature[3)]. Our simulations for even higher densities reveal the formation of an ionic lattice immersed into a delocalized sea of electrons, i.e., an ionic Wigner crystal [40], known to exist in high-density objects such as white or brown dwarf stars. Thus, qualitatively, the simulations show the correct behavior at high densities. But because of the small size of the simulations (only 50 electrons and protons are presently feasible), the results are much closer to those for small strongly correlated ionic clusters that are known to exhibit quite peculiar behavior, including strong size dependence of the energy, negative specific heat, etc. In order to obtain more accurate data for the internal energy of a macroscopic two-component plasma at ultrahigh compression, a significant increase of the simulation size is therefore desirable (it should become feasible in the near future).

B) The energy minimum at intermediate densities is reproduced by all methods, but there are quantitative differences regarding its depth and width. The general observation made for all temperatures, cf. Figs. 1–3, is that the simulations yield a deeper minimum and shift of the energy increase towards higher densities. We also observe that the EIIP method yields lower energies than the PACH and is closer to the DPIMC results. Further, the PACH results practically coincide with the DFT data [46] where they are available ($T = 10000$ K and $n \geq 5 \cdot 10^{23}$ cm^{-3}). But atom and molecule formation is becoming important at these densities, and the EIIP and DFT methods (in their present form) are becoming increasingly unreliable. The presented PACH results include bound states approximately, whereas the DPIMC calculations have no restrictions with re-

[3)] In fact, the first minimum of the proton-proton function (around $r = 0.45a_B$) for $T = 10000$ K is far lower than the standard value of 0.35 typical for a liquid.

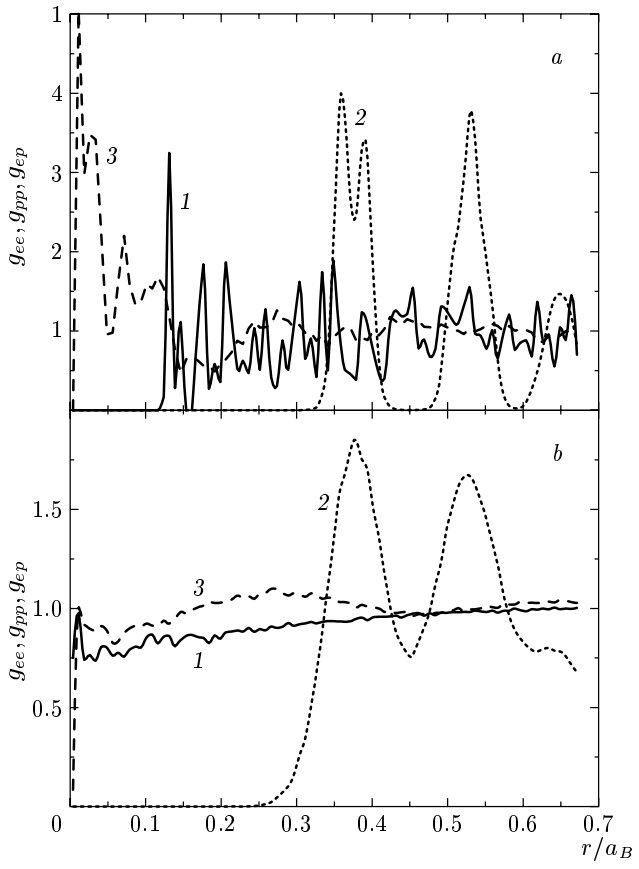

Fig. 4. Electron–electron (*1*), proton–proton (*2*) and electron–proton (*3*) pair distribution functions of hydrogen from the DPIMC simulations at $n = 10^{26}$ cm^{-3} for the temperatures 10000 K (*a*) and 50000 K (*b*). Note the different vertical scales

spect to atom and molecule formation.

We now analyze the DPIMC simulations around the energy minimum. Our data for $T = 10000$ K are also significantly lower than RPIMC results of Militzer et al. [34], cf. Fig. 1*b*, but we found excellent quantitative agreement between the two independent quantum Monte Carlo methods above $T = 50000$ K, see the point for $T = 62500$ K in Fig. 3*a* (a more extensive comparison is also given in Ref. [42]). A detailed analysis of the DPIMC simulation results at $T = 10000$ K and 10^{23} cm$^{-3} \lesssim n \lesssim 10^{24}$ cm^{-3} revealed that the homogeneous plasma state is unstable there: the plasma gains energy by forming higher-density clusters or droplets that are embedded into a lower density plasma. The droplets are clearly visible in the electron–proton configurations in the simulation box [68] and are interpreted as a direct indication for a first-order phase transition, as discussed in the Introduction [13–20]. These effects emerge in the weakly ionized plasma (low density) and vanish above the Mott point, $r_s \sim 1$. We mention that the same effects are observed in our DPIMC simulations of electron–hole plasmas under similar conditions [69], for which droplet formation is well established and was observed experimentally three decades ago [70]. Our conclusion is also indirectly supported by analytic methods. In the present variants of the PACH and EIIP methods, homogeneous density distributions are assumed[4)], but it is interesting that at $T = 10000$ K and 10^{23} cm$^{-3} \lesssim n \lesssim 10^{24}$ cm^{-3}, both methods yield unstable results for the thermodynamic functions, which is a clear indication of the existence of a first-order phase transition. Xu and Hansen [46] also observed strong fluctuations in their density functional calculations below $r_s = 1.5$, which they found to strongly resemble precursors of a phase transition.

Even if we accept the existence of a phase transition, the energy obtained in the DPIMC simulations appears to be unexpectedly low. In this region, we observe large fluctuations of pressure and energy related to the formation and decay of droplets. Furthermore, there are significant surface energy effects. Our simulations yield only a very small number of droplets (typically one to three), each containing 15 to 50 electron–proton pairs. Of these, almost all are on the surface[5)]. We cannot therefore be certain that our simulations adequately represent a macroscopic system in the two-phase region and its energy per particle in particular. Finally, in such small systems, there exist additional specific factors that tend to lower the energy [12] and can therefore be responsible for our result. This can also be the reason for the low-energy minimum observed at higher temperatures, Figs. 2 and 3, where our analytic models do not show unstable behavior. Clarifying this interesting issue in more detail requires performing extensive simulations with substantially larger particle numbers; such calculations are presently under way.

C) In the region to the left of the energy minimum, $n \lesssim 10^{22}$ cm^{-3}, the simulations are of special importance. In this region, the plasma is strongly correlated and largely dominated by bound states. Analytic methods based on perturbation expansions in the coupling strength (Γ or r_s) do not work in this parameter range.

[4)] Using a modified PACH approach, Beule et al. [20] predicted a first order phase transition in hydrogen for $T = 10000$ K with a pressure and density $p \approx 110$GPa and $\rho \approx 0.8$ g $\cdot$ cm^{-3}. Similar results were obtained by Schlanges et al. [16] where also other references are given.

[5)] Imagine 27 (64) particles arranged, for simplicity, in a small cube. Evidently, 26 (56) of them will be situated at the surface of the «droplet» which is in striking contrast to the situation of a macroscopic system where droplets are expected to contain many orders of magnitude more particles.

While there exist many chemical models of various degress of sophistication, rigorous theoretic results are very rare. In particular, as mentioned above, the EIIP model breaks down here (we recall that its present version is limited to $r_s \leq 1.5$, cf. Sec. 3). Also, the present version of the PACH approach uses a chemical picture with a nonideal Saha equation, but treats bound states in a very simple approximation (see above) and therefore yields only approximate results in situations with a low ionization degree. In contrast, the DPIMC results have no such limitations and provide reliable results in this region in principle. On the other hand, there exist specific technical difficulties at low densities, where the extension of bound electron wave functions is many orders of magnitude smaller than the interparticle distance, which leads to very slow convergence of DPIMC simulations (and other quantum Monte Carlo methods as well). This explains the different energies of the DPIMC and Padé results at the lowest densities at $T = 10000$ K, where the plasma consists of atoms, see, e.g., [16, 20], while good agreement is found at higher temperatures.

7. DISCUSSION

This work is devoted to the investigation of the total energy of warm dense plasmas in the temperature range between 100000 and 50000 K. We presented a new theoretic approach to high-density plasmas based on the theory of an effective ion–ion potential. This method was shown to be quite efficient for fully ionized strongly correlated plasmas above the Mott density. Furthermore, a detailed comparison of several theoretic approaches and simulations was performed over a wide density range. The first included the EEIP and PACH analytic models on the one hand and recent DFT data of Xu and Hansen [46] on the other hand. The second group of data consisted of several new data points based on DPIMC simulations of a correlated proton–electron system with degenerate electrons. From these comparisons, we conclude that the three theoretic approaches — PACH, EEIP, and DFT — are in a very good agreement with each other for a fully ionized hydrogen plasma in the high-density region where $r_s < 1$. We therefore expect these results to be reliable for densities above $3 \cdot 10^{24}$ cm^{-3}. This agreement of the three independent analytic methods is highly interesting because the physical approximations involved are very different. On the other hand, our DPIMC simulations agree with the available RPIMC data for temperatures above 50000 K, cf. Figs. 1–3 and Ref. [42]. This agreement over a broad range of parameters is certainly remarkable because the plasma is far outside the perturbative regime: it is strongly correlated and the electrons are degenerate, and the two simulations are essentially independent.

The comparison of our DPIMC simulation results with the analytic data reveals an overall good agreement. In addition, existing deviations are a useful guide for future improvement and extension of the various approaches. Most importantly, the good quality of the quantum Monte Carlo data in the region of strong changes of the ionization degree fill a gap in the present variants of analytic methods. These data can be used to improve the treatment of a dense plasma in analytic methods in the theoretically very complicated region of strong correlations and strongly varying ionization and dissociation degrees. Moreover, the high-density asymptotic results of the analytic methods may be useful for further improvement of the simulations.

Further, our DPIMC simulations revealed an instability of the homogeneous plasma state around the minimum of the energy isotherm $T = 10000$ K for densities between 10^{23} and 10^{24} cm^{-3}. We have given arguments that this is related to droplet formation, which is a strong indication of a first-order phase transition [68] that has previously been predicted by many authors on the basis of simple chemical models. The existence of a plasma phase transition would have drastic consequences for transport properties of many astrophysical objects, such as the giant planets, and its verification therefore remains an important theoretical issue. It would therefore be very interesting if independent first-principle simulations, in particular RPIMC, could reproduce this result. This, however, may require a particular choice of nodes of the density matrix that allow an inhomogeneous equilibrium plasma state. Finally, at very high-densities, our DPIMC simulations revealed ordering of protons into a strongly correlated fluid and the onset of the formation of a proton Wigner crystal. These interesting physical effects in high pressure hydrogen are of relevance for many astrophysical systems and many laboratory experiments, including ultracold degenerate trapped ions and laser plasmas.

In conclusion, we may state that the analytic methods and the DPIMC approach are already in a reasonable overall agreement. Both methods should be developed to further explore the equilibrium properties of dense hydrogen.

We acknowledge stimulating discussions with H. E. DeWitt, W. D. Kraeft, D. Kremp, B. Militzer, R. Redmer, and M. Schlanges. This work has been

supported by the Deutsche Forschungsgemeinschaft (BO-1366) and by a grant for CPU time at the NIC Jülich.

REFERENCES

1. *Strongly Coupled Coulomb Systems*, ed. by G. Kalman, Pergamon Press, New York (1998).
2. *Proc. Int. Conf. on Strongly Coupled Plasmas*, ed. by W. D. Kraeft and M. Schlanges, World Scientific, Singapore (1996).
3. W. D. Kraeft, D. Kremp, W. Ebeling, and G. Röpke, *Quantum Statistics of Charged Particle Systems*, Akademie-Verlag, Berlin (1986).
4. M. Bonitz and B. G. Teubner, *Quantum Kinetic Theory*, Stuttgart/Leipzig (1998).
5. *Proc. 10th Int. Workshop on the Physics of Nonideal Plasmas*, ed. by H. Haberland, M. Schlanges, and W. Ebeling, Contr. Plasma Phys. **41**(2–3), (2001).
6. *Progress in Nonequilibrium Green's Functions*, ed. by M. Bonitz, World Scientific, Singapore (2000).
7. L. B. Da Silva et al., Phys. Rev. Lett. **78**, 483 (1997).
8. S. T. Weir, A. C. Mitchell, and W. J. Nellis, Phys. Rev. Lett. **76**, 1860 (1996).
9. E. P. Wigner and H. B. Huntington, J. Chem. Phys. **3**, 764 (1935).
10. A. A. Abrikosov, Zh. Eksp. Teor. Fiz. **39**, 1798 (1960); **41**, 565 (1961); **45**, 2038 (1962).
11. N. W. Ashcroft and D. Stroud, in *Solid State Physics*, ed. by H. Ehrenreich, F. Seitz, and D. Turnbull, Academic New York, v. 33, p. 1; N. W. Ashcroft, Phys. Rev. Lett. **21**, 1748 (1968).
12. E. G. Brovman, Yu. Kagan, and A. Kholas, Zh. Eksp. Teor. Fiz. **61**, 2429 (1971).
13. G. E. Norman and A. N. Starostin, Teplofiz. Vys. Temp. **6**, 410 (1968); **8**, 413 (1970).
14. P. Haronska, D. Kremp, and M. Schlanges, Wiss. Z. Universität Rostock **98**, 1 (1987).
15. D. Saumon, and G. Chabrier, Phys. Rev. A **44**, 5122 (1991).
16. M. Schlanges, M. Bonitz, and A. Tschttschjan, Contrib. Plasma Phys. **35**, 109 (1995).
17. W. Ebeling, W. D. Kraeft, and D. Kremp, *Theory of Bound States and Ionization Equilibrium in Plasmas and Solids*, Akademie-Verlag, Berlin (1976).
18. W. Ebeling, Physica A **130**, 587 (1985).
19. W. Ebeling and W. Richert, Phys. Lett. A **108**, 80 (1985); Phys. Stat Sol. (b) **128**, 167 (1985).
20. D. Beule et al., Phys. Rev. B **59**, 14177 (1999); Contr. Plasma Phys. **39**, 21 (1999).
21. V. M. Zamalin, G. E. Norman, and V. S. Filinov, *The Monte Carlo Method in Statistical Thermodynamics*, Nauka, Moscow (1977); B. V. Zelener, G. E. Norman, and V. S. Filinov, *Perturbation Theory and Pseudopotential in Statistical Thermodynamics*, Nauka, Moscow (1981).
22. J.-P. Hansen and P. Viellefosse, Phys. Lett. A **53**, 187 (1975); S. Galam and J. P. Hansen, Phys. Rev. A **14**, 816 (1976).
23. H. E. De Witt, in *Strongly Coupled Plasmas*, ed. by G. Kalman and P. Carini, Plenum, New York (1978).
24. N. P. Kovalenko, Yu. P. Krasny, and S. A. Trigger, *Statistical Theory of Liquid Metals*, Nauka, Moscow (1990).
25. M. Bonitz et al., J. Phys. B: Condensed Matter **8**, 6057 (1996).
26. V. Golubnychiy, M. Bonitz, D. Kremp, and M. Schlanges, Phys. Rev. E **64**, 016409 (2001).
27. W. Ebeling, W. Stolzmann, A. Förster, and M. Kasch, Contr. Plasma Phys. **39**, 287 (1999).
28. D. Klakow, C. Toepffer, and P.-G. Reinhard, Phys. Lett. A **192**, 55 (1994); J. Chem. Phys. **101**, 10766 (1994).
29. *The Monte Carlo and Molecular Dynamics of Condensed Matter Systems*, ed. by K. Binder and G. Ciccotti, SIF, Bologna (1996).
30. *Classical and Quantum Dynamics of Condensed Phase Simulation*, ed. by B. J. Berne, G. Ciccotti, and D. F. Coker, World Scientific, Singapore (1998).
31. D. M. Ceperley, in Ref. [29], p. 447.
32. D. M. Ceperley, Rev. Mod. Phys. **65**, 279 (1995).
33. B. Militzer and E.L. Pollock, Phys. Rev. E **61**, 3470 (2000).
34. B. Militzer and D. M. Ceperley, Phys. Rev. Lett. **85**, 1890 (2000).
35. V. S. Filinov, J. Phys. A **34**, 1665 (2001).
36. M. Imada, J. Phys. Soc. Jap. **53**, 2861 (1984).
37. M. F. Herman, E. J. Bruskin, and B. J. Berne, J. Chem. Phys. **76**, 5150 (1982).

38. V. S. Filinov, P. R. Levashov, V. E. Fortov, and M. Bonitz, in Ref. [6], p. 513; E-print archives cond-mat/9912055.

39. V. S. Filinov and M. Bonitz, E-print archives cond-mat/9912049.

40. V. S. Filinov, M. Bonitz, and V. E. Fortov, Pis'ma v Zh. Eksp. Teor. Fiz. **72**, 245 (2000).

41. V. S. Filinov, V. E. Fortov, M. Bonitz, and D. Kremp, Phys. Lett. A **274**, 228 (2000).

42. V. S. Filinov, M. Bonitz, W. Ebeling, and V. E. Fortov, Plasma Phys. Contr. Fusion **43**, 743 (2001).

43. W. Ebeling, Ann. Physik (Leipzig) **21**, 315 (1968); **22**, 33, 383, 392 (1969); Physica **38**, 378 (1968); **40**, 290 (1968).

44. W. Ebeling, Contr. Plasma Physics **29**, 165 (1989); **30**, 553 (1990).

45. W. Ebeling, A. Förster, V. Fortov, V. Gryaznov, and A. Polishchuk, *Thermophysical Properties of Hot Dense Plasmas*, Teubner, Stuttgart–Leipzig (1991).

46. H. Xu and J. P. Hansen, Phys. Rev. E **57**, 211 (1998).

47. F. J. Dyson, and A. Lenard, J. Math. Phys. **8**, 423 (1967).

48. E. H. Lieb and W. Thirring, Phys. Rev. Lett. **31**, 111 (1975).

49. E. Wigner, Phys. Rev. **46**, 1002 (1934).

50. W. A. Harrison, *Pseudopotentials in the Theory of Metals*, W. A. Benjamin, INC., New York/Amsterdam (1966).

51. V. B. Bobrov and S. A. Trigger, Sol. St. Comm. **56**, 21, 27 (1985).

52. S. D. Kaim, N. P. Kovalenko, and E. V. Vasiliu, J. Phys. Studies **1**, 589 (1977).

53. G. Mahan, *Many-Particle Physics*, Plenum Press, New York (1981).

54. S. Hamaguchi, R. T. Farouki, and D. H. E. Dubin, Phys. Rev. E **56**, 4671 (1997).

55. R. T. Farouki and S. Hamaguchi, J. Chem. Phys. **101**, 9885 (1994).

56. T. Kahlbaum, in *Physics of Strongly Coupled Plasmas*, ed. by W. D. Kraeft and M. Schlanges, World Scientific, Singapore (1996).

57. W. Ebeling, W. D. Kraeft, D. Kremp, and G. Röpke, Physica A **140**, 160 (1986).

58. W. L. Slattery, G. D. Doolen, and H. E. De Witt, Phys. Rev. A **21**, 2087 (1980).

59. R. P. Feynman and A. R. Hibbs, *Quantum Mechanics and Path Integrals*, McGraw-Hill, New York (1965).

60. V. S. Filinov, High Temperature **13**, 1065 (1975); **14**, 225 (1976).

61. B. V. Zelener, G. E. Norman, and V. S. Filinov, High Temperature **13**, 650 (1975).

62. G. Kelbg, Ann. Physik **12**, 219 (1963); **13**, 354; **14**, 394 (1964).

63. W. Ebeling, H. J. Hoffmann, and G. Kelbg, Contr. Plasma Phys. **7**, 233 (1967) and references therein.

64. A. V. Filinov, Yu. E. Lozovik, and M. Bonitz, Phys. Stat. Sol. (b) **221**, 231 (2000).

65. A. V. Filinov, M. Bonitz, and Yu. E. Lozovik, Phys. Rev. Lett. **86**, 3851 (2001).

66. S. A. Trigger and W. Ebeling, *Proc. of the IInd Capri Workshop on Dusty Plasmas*, Capri (2001).

67. N. I. Klyuchnikov and S. A. Trigger, Dokl. of Russian Academy of Science **238**, 565 (1978).

68. V. S. Filinov, V. E. Fortov, M. Bonitz, and P. R. Levashov, Pis'ma v Zh. Eksp. Teor. Fiz. **74**, 422 (2001).

69. V. S. Filinov, W. Hoyer, M. Bonitz, and S. W. Koch, private communication.

70. *Electron-hole Droplets in Semiconductors*, ed. by C. D. Jeffries, and L. V. Keldysh, Nauka, Moscow (1988); J. C. Hensel, T. G. Phillips, and G. A. Thomas, Sol. St. Phys. **32**, 88 (1977).